On the effect of current pulses on the material behavior during electromagnetic metal forming *

J. Unger[1], M. Stiemer[2], L. Walden[3], F. Bach[3], H. Blum[2], B. Svendsen[1]

[1] Chair of Mechanics, University of Dortmund, Germany
[2] Chair of Scientific Computing, University of Dortmund, Germany
[3] Institute of Material Technology, University of Hannover, Germany

Abstract

Electromagnetic sheet metal forming (EMF) is an example of a high-speed forming process driven by the dynamics of a coupled electromagnetic-mechanical system. Basic physical processes involved in EMF, such as e.g. inelastic and hardening behavior or inertia, have been considered in previous works [1, 2]. The purpose of the current work is the investigation of temperature development during EMF and a possible reduction in the yield stress due to electric currents. While thermoelastic and viscoplastic effects are well-understood in this context [3], the possible influence of electric currents on dislocation motion, generally referred to as the electro-plastic effect [4, 5], is still an unresolved issue. In agreement with previous works [e.g., 6], it is concluded here that such an effect is at most of second-order and can most likely be safely neglected in the modeling and simulation of industrial EMF.

Keywords:

Electromagnetic metal forming, Electroplasticity, Magneto-thermo-inelastic coupling

1 Introduction

In electromagnetic metal forming (EMF) a strong pulsed magnetic field generated in the tool coil adjacent to an electrically-conducting workpiece induces eddy currents in the workpiece, which interact with the magnetic field, inducing, in turn, a Lorentz (body) force (density) in the work-piece which drives the forming process. The entire forming process takes approximately

[*] *This work was carried out in the context of the German Research Foundation (Deutsche Forschungsgemeinschaft (DFG)) Research Group FOR 443. The authors wish to thank the DFG for its financial support.*

100-300 μs and achieves strain-rates of up to 10^4 s^{-1}. Compared to other forming methods, it offers increased formability for certain kinds of materials, reduction in wrinkling, the possibility of combining forming and assembly operations, reduced tool-making costs *etc.*. An example of the basic experimental setup for the case of sheet metal forming is shown in Figure 1. The time-dependent current in the tool coil shown on the right in this figure depicts the pulsed nature of this current and, thus, of the resulting magnetic field.

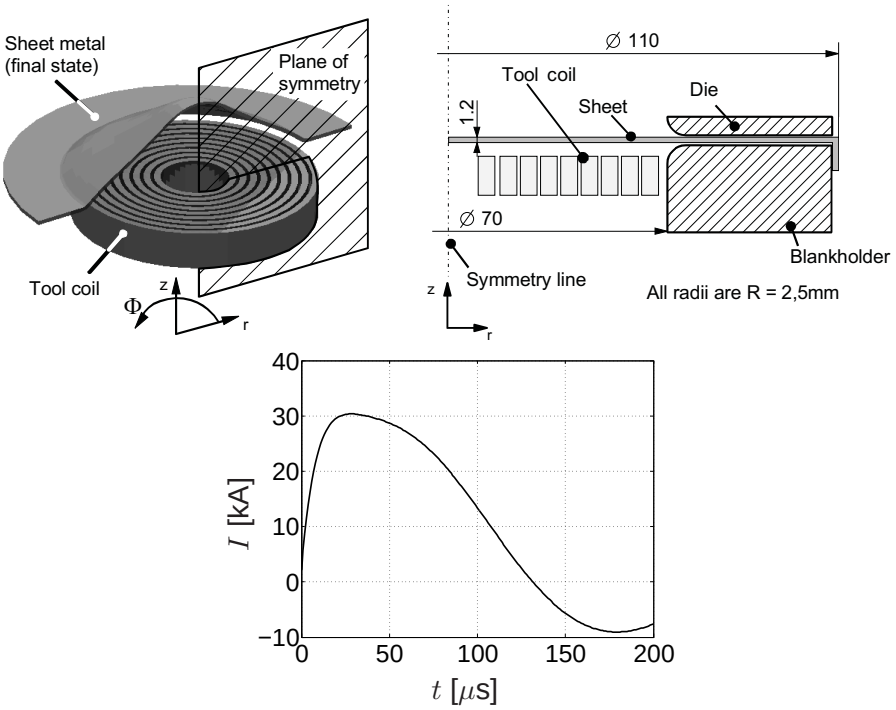

Figure 1: *Electromagnetic sheet metal forming setup*

The further development of EMF as an industrial forming process depends in particular on the availability and use of reliable simulation tools for the corresponding coupled multifield problem. In particular, these must be able to deal with high strain rates $\dot{\epsilon} \geq 10^4$ s^{-1}, large current densities $|\boldsymbol{j}| \geq 10^4$ A/mm^2, and strong magnetic fields $|\boldsymbol{b}| \geq 10^0$ T. In this context, we examine possible effects in the material such as a reduction in yield stress due to temperature and/or strong electrical currents. In the literature, the electroplastic (EP) effect has been postulated to contribute to the behavior of metals under combined mechanical and electromagnetic loading [7, 8]. Here, the idea is that an interaction between the electric current and dislocations may affect the hardening behavior and, in particular, the yield stress. There has been a considerable debate regarding the significance of such an effect in polycrystal metals [9]. Figure 2 shows the current density and tensile test response of an experiment performed by Okazaki *et al.* [10]. In their experiment, a titanium bar with diameter d = 0.511 mm was loaded in simple tension. As shown in Figure 2, the discharge of a capacitor bank at given times during this loading resulted in a sudden increase in the current density and the time-correlated drop in the yield stress. Okazaki *et al.* [10] showed that each of these current-density "jumps" resulted in a temperature rise of about 12.2 K to 99.9 K, depending on the imposed current density. Since a temperature rise of this order of magnitude implies a drop of the yield stress of about 0.4%

and 5.0%, authors favoring the electroplastic effect concluded that the observed drops are due to an interaction of electron movements and the moving dislocations.

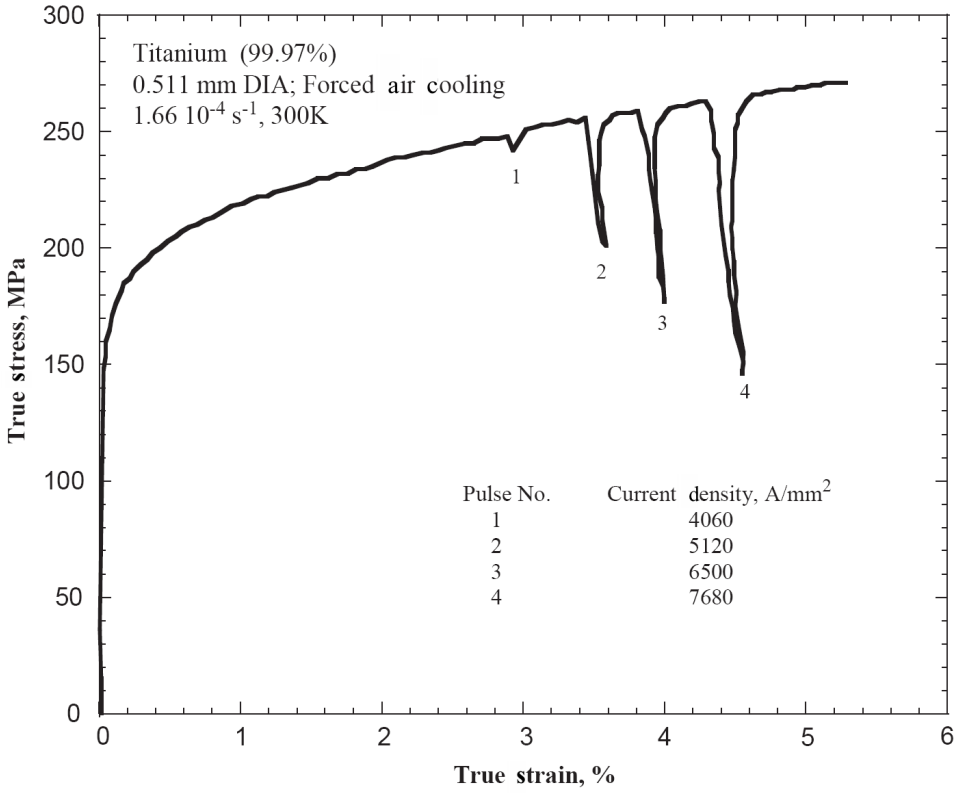

Figure 2: *Experimental results of Okazaki et al. [10]. During tensile testing of a circular bar an imposed current density results in stress drops. The current density achieved maximum values of 4060 to 7680 A/mm^2 and lasted for about 60 μs. For pulse no. the 2 tensile stress decreased to about 70% of its original value.*

Recently, Bilyk *et al.* [6] showed that the introduction of an EP effect is not necessary to explain the stress drops shown in Figure 2. Bilyk *et al.* [6] concluded that the stress drops can be modeled by an accurate modeling of viscoplastic rate effects during pulsing. The work presented here confirms the view that the stress drops can be explained with the help of conventional effects like Joule heating, thermal expansion, and viscoplasticity. In particular, we focus here on thermal expansion.

2 Thermoelastic, viscoplastic model including Joule heating

The multifield material model used in the current work represents a special case of the general continuum thermodynamic formulation of such models from Svendsen & Chanda [1] to the formulation of models for electromagnetic thermoelastic, viscoplastic solids. In particular, this work provides a framework for the treatment of EMF processes also accounting for the interaction between the electromagnetic and thermomechanical effects at *large* deformation. The case of the simple tension tests mentioned above is somewhat simpler than the one of sheet

metal forming shown in Figure 1 in the sense that the total strain is significantly smaller ($\approx$ 5%). According to Svendsen & Chanda [1], the magnetic field can be modeled as diffusive over the length- and timescales of interest. In this case, Maxwell's equations and Ohm's law yield the diffusive field relation

$$\mathbf{0} = \partial \boldsymbol{b} - \kappa_{\text{EM}} \, \nabla^2 \boldsymbol{b} \tag{1}$$

for the spatial magnetic flux density $\boldsymbol{b}$. Here, $\kappa_{\text{EM}} \coloneqq \sigma_{\text{EM}}^{-1} \mu_{\text{EM}}^{-1}$ represents the magnetic diffusivity, μ_{EM} the magnetic permeability, and σ_{EM} the electric permittivity. (Note that all material and modeling data can be found in Tables 2 and 3 as well as in §2). In particular, on a timescale τ, κ_{EM} implies a skin depth (*i.e.*penetration depth of the magnetic field into the material) of $\ell_{\text{EM}} = \sqrt{\kappa_{\text{EM}} \tau}$. As indicated in Table 1, for the case of titanium the skin depth is significantly larger than the radius of the "bar" (*i.e.*, a wire here). Consequently, the current density is in the wire. For a long wire (*i.e.*, $l/r_0 \gg 1$), (1) can be solved to obtain

$$(b_r, b_\varphi, b_z)(r) = (0, \frac{\sigma_{\text{EM}} I r}{2\pi r_0^2}, 0) \tag{2}$$

in cylindrical coordinates (r, φ, z) [11]. Here I represents the imposed current, and r_0 the radius of the wire. In turn, this implies a constant current density

$$(j_r, j_\varphi, j_z)(r) = (0, 0, I/\pi r_0^2) \tag{3}$$

within the cross-section of the wire.

Next, consider the energy balance and temperature evolution in the bar. Here, the chacteristic lengthscale is determined as usual by the thermal diffusivity $\kappa_{\text{TM}} \coloneqq k_r/\varrho_r c_r$, where k_r represents the thermal conductivity, c_r the specific heat capacity, and ϱ_r the mass density at reference temperature θ_r. As usual, on a timescale τ significant thermal conduction will take place on the lengthscale $\ell_{\text{TM}} = \sqrt{\kappa_{\text{TM}} \tau}$. Since this lengthscale is much smaller than the width of the wire (see Table 1), we are justified in assuming adiabatic conditions over the timescale of the pulses ($\leq$ 100 μs). Over longer timescales, of course, this is not the case. Finally, in contrast to EMF we neglect the radially acting Lorentz force for two reasons: firstly, its magnitude is significantly smaller than the applied mechanical loads [6] and, secondly, due to the geometric conditions the structural response is minimal.

	ℓ_{EM}/r_0	ℓ_{TM}/r_0
Al	5.8×10^0	4.0×10^{-1}
Ti	2.2×10^1	1.2×10^{-1}
Assumption	Uniform current density	Adiabatic during pulsing

Table 1: *Scaling relations for electromagnetic diffusion and thermal diffusion*

With these simplifications the temperature is homogeneous and treated as an internal variable (see $(10)_3$ below). Consequently, the deformation $\boldsymbol{\xi}$ is the only thermomechanical field, given as usual by the weak form

$$\int_{B_{\text{r}}} \varrho_r \, \ddot{\boldsymbol{\xi}} \cdot \boldsymbol{\xi}_* + \boldsymbol{K} \cdot \nabla \boldsymbol{\xi}_* = 0 \tag{4}$$

for pure kinematic boundary conditions with respect to the reference configuration B_r for all corresponding test fields $\boldsymbol{\xi}_*$. Here, $\boldsymbol{K}$ represents the Kirchhoff stress. As usual, this latter variable, along with the internal variables, is given by a material model. For simplicity, attention is resticted here to the case of (isotropic) thermoelastoviscoplasticity with isotropic hardening. Further, in the case of metals, we have small elastic strain. The relevant internal variables are then the elastic left logarithmic stretch $\ln\boldsymbol{V}_E$ and the accumulated inelastic strain ϵ_P. On this basis, the thermodynamic formulation being pursued here is based on specific model relations for the referential free energy density ψ as well as on the evolution relations for the internal variables. In particular, assuming for simplicity that the elastic behavior is not affected by inelastic processes such as damage, the split

$$\psi(\theta, \ln\boldsymbol{V}_E, \epsilon_P) = \psi_E(\theta, \ln\boldsymbol{V}_E) + \psi_P(\theta, \epsilon_P) \tag{5}$$

of the free energy into thermoelastic and inelastic parts is justified [*e.g.*, 12]. Assuming for simplicity that the specific heat capacity c_r is constant [13] and exploiting the condition of small elastic strain, one obtains the thermoelastic neo-Hooke form

$$\begin{aligned} \psi_E(\theta, \ln\boldsymbol{V}_E) &= \tfrac{1}{2}\,\lambda_r\,(\boldsymbol{I}\cdot\ln\boldsymbol{V}_E)^2 - (3\lambda_r + 2\mu_r)\,\alpha_r(\theta-\theta_r)\,(\boldsymbol{I}\cdot\ln\boldsymbol{V}_E) + \tfrac{1}{2}\,\mu_r(\ln\boldsymbol{V}_E\cdot\ln\boldsymbol{V}_E) \\ &+ \varrho_r c_r\,[\theta-\theta_r-\theta\ln(\theta/\theta_r)] \end{aligned} \tag{6}$$

for ψ_E, where λ_r and μ_r represent Lamé's constants and α_r the thermal heat expansion coefficient. The inelastic part ψ_P is determined empirically with the help of experimental data, as discussed in the next section. Next, consider the evolution of the internal variables and the inelastic behavior. In the metallic polycrystalline materials of interest at low-to-moderate homologous temperature, inelastic deformation processes are controlled predominantly by the activation of dislocation glide on glide systems (*e.g.*, [14]), even at higher strain-rates. As such, higher homologous temperatures are required for other mechanisms such as dislocation climb or even dynamic recrystallization to activate. Resistance to dislocation glide arises due to extended obstacles generating longer-range stress fields related in the phenomenological context to hardening behavior. In addition, such resistance is caused by short-range local obstacles which can be overcome by thermal fluctuation under the action of local effective stress, represented in the current phenomenological context by $|\mathrm{dev}(\boldsymbol{K})| + \varsigma_P - \sigma_{F0}(\theta)$, where

$$-\varsigma_P \coloneqq \psi_{,\epsilon_P} \tag{7}$$

represents the static contribution to the flow stress (in shear). On this basis,

$$f_P \coloneqq \frac{|\mathrm{dev}(\boldsymbol{K})| + \varsigma_P}{\sigma_P} \tag{8}$$

represents an activation function or non-dimensional overstress in the current rate-dependent context. Here, σ_P represents the dynamic drag contribution to the effective flow stress in the system. On this basis, a power-law approximation of the more exact transition-state-based micromechanical relations for the kinetics of dislocation glide leads to the power-law form

$$\phi = \frac{\gamma_P\,\sigma_P}{m_P+1}\,\langle f_P\rangle^{m_P+1} \tag{9}$$

upon which the evolution of the internal variables is based. Here, γ_{P} represents a characteristic strain-rate, $\langle x\rangle := \frac{1}{2}(x+|x|)$ the MaCauley bracket, and m_{P} the strain-rate exponent. In general, these will be functions of temperature and rate of deformation; here, we treat them for simplicity as constants. This potential determines as usual the forms

$$\begin{aligned} \ln^{*}\boldsymbol{V}_{\text{E}} &= -\phi_{,\boldsymbol{K}} &&= -\operatorname{sgn}(\operatorname{dev}(\boldsymbol{K}))\,\dot{\epsilon}_{\text{P}} \quad (\boldsymbol{K}\neq\boldsymbol{0})\,, \\ \dot{\epsilon}_{\text{P}} &= \phi_{,\varsigma_{\text{P}}} &&= \gamma_{\text{P}}\,\langle f_{\text{P}}\rangle^{m_{\text{P}}} \quad (f_{\text{P}}>0)\,, \\ \dot{\theta} &= \varrho_r^{-1}c_r^{-1}\{\omega_r+\sigma_{\text{EM}}^{-1}\det(\boldsymbol{F})\,\boldsymbol{j}\cdot\boldsymbol{j}\} &&\quad , \end{aligned} \tag{10}$$

for the evolution of the internal variables. Here, ω_r represents the rate of mechanical heating and $\sigma_{\text{EM}}^{-1}\boldsymbol{j}\cdot\boldsymbol{j}$ the electromotive power.

Now, for the case of incompressible material behavior, we assume that the isotropic forms of the viscoplastic parameters γ_{P}, σ_{P}, and m_{P} are independent of the trace $\boldsymbol{I}\cdot\boldsymbol{D}$ of the rate of deformation. In this case, the thermoelastic form

$$\boldsymbol{K} = \psi_{,\ln\boldsymbol{V}_{\text{E}}} = \{\lambda_r\,(\boldsymbol{I}\cdot\ln\boldsymbol{V}_{\text{E}}) - (3\lambda_r+2\mu_r)\,\alpha_r(\theta-\theta_r)\}\boldsymbol{I} + \mu_r\ln\boldsymbol{V}_{\text{E}} \tag{11}$$

for the Kirchhoff stress holds from (6). In addition,

$$\omega_r = \gamma_{\text{P}}\,\sigma_{\text{P}}\langle f_{\text{P}}\rangle^{m_{\text{P}}+1} - (3\lambda_r+2\mu_r)\,\alpha_r\,\theta\,\dot{\overline{\ln\det(\boldsymbol{F})}} \tag{12}$$

then follows for the referential form of the mechanical heating rate.

This completes the basic model formulation. The detailed algorithmic formulation and numerical implementation of the finite-element-model has been presented in Stiemer *et al.* [2]. In particular, note that the time-step size for tensile test simulation has to be chosen according to the particular time scale where changes of internal variables are to be expected. During current pulses the time-step size was chosen to be 10^{-6} s. Otherwise, much larger step sizes on the order of 10^{0} s were chosen. The time integration of the velocity and acceleration fields was carried out using Newmark's method. Numerical damping was applied during pulsing and afterwards in order to avoid unphysical oscillations.

3 Application to metal bars subject to pulsed currents and simple tension

In this section, the current model is applied to the tensile tests with pulsed electric currents. To this end, we specify the semi-analytical form

$$-\varsigma_{\text{P}} = \psi_{,\epsilon_{\text{P}}} = \sigma_{\text{F0}}\left(1+\frac{\epsilon_{\text{P}}}{\epsilon_0}\right)^{n} - \sigma_{\text{F0}} \tag{13}$$

for the strain hardening due to energy storage, with

$$\sigma_{\text{F0}} = \sigma_{\text{F0}r}(1-\omega_{\text{TM}}(\theta-\theta_r)) \tag{14}$$

of the initial static flow stress, $\sigma_{\text{F0}r}$ being the initial flow stress at reference temperature θ_r. The parameter ω_{TM} mediates the reduction of the initial flow stress due to an increase of the

temperature. Table 2 summarizes the material parameters characterizing the inelastic material behavior. For titanium, the parameters in (13) were obtained from Bilyk *et al.* [6]. In particular, ω_{TM}, γ_{P}, σ_{P}, and m_{P} were fitted to the model data also provided in Bilyk *et al.* [6]. For aluminum, the tensile test data were used for the strain hardening fit. Table 3 lists the remaining material parameter values needed.

	$\sigma_{\mathrm{F}0r}$ MPa	ϵ_0 -	n -	ω_{TM} K^{-1}	γ_{P} s^{-1}	σ_{P} MPa	m_{P} -
Al	3.5×10^1	2.0×10^{-3}	1.9×10^{-1}	1.4×10^{-3}	1.0×10^{-4}	5.0×10^0	4.0×10^0
Ti	1.7×10^2	2.0×10^{-3}	1.5×10^{-1}	8.7×10^{-4}	1.0×10^{-4}	4.0×10^0	4.0×10^0

Table 2: *Inelastic parameters*

	λ_r MPa	μ_r MPa	α_r K^{-1}	ϱ_r kg m^{-3}	c_r m s^{-2} K^{-1}	k_r J s^{-1} m^{-1} K^{-1}
Al	5.0×10^4	2.6×10^4	2.3×10^{-5}	2.7×10^3	9.2×10^8	2.4×10^2
Ti	8.5×10^4	4.4×10^4	8.6×10^{-6}	4.5×10^3	5.2×10^8	2.2×10^1

Table 3: *Thermoelastic parameters*

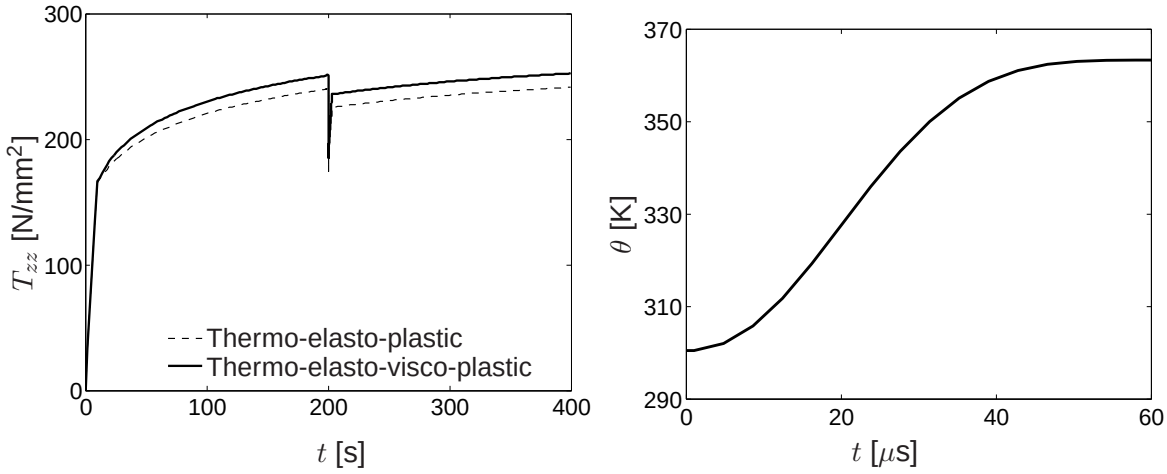

Figure 3: *Current pulse applied to a titanium bar undergoing simple tension. Left: Development of the zz-component of the Cauchy stress simulated with a thermoelastic, viscoplastic model (rate-dependent: solid line) and a thermoelastic, elastoplastic model (rate-independent: dashed line). Right: Temperature rise from Joule heating during the current pulse starting at t = 200s*

Next, consider the results in Figure 3 for the case of a current pulse applied to a titanium bar undergoing simple tension in the z-direction. At the time of the pulse (t = 200 s), Joule heating results in a temperature rise from 301 K to 363 K in 60 μs. The slight temperature rise of 3 K before the pulse is due to mechanical dissipation. In the left part of Figure 3, the change in the zz-component of the Cauchy stress $\boldsymbol{T} = J^{-1}\boldsymbol{K}$ as a function of time is shown. As can be seen, the current pulse results in a reduction of this component. In addition, both the rate-dependent and rate-independent cases show this change. In contrast to the work of Bilyk *et*

al. [6], we claim that not the rate effect, but rather the thermal expansion effect is crucial to correctly model the observed stress drop.

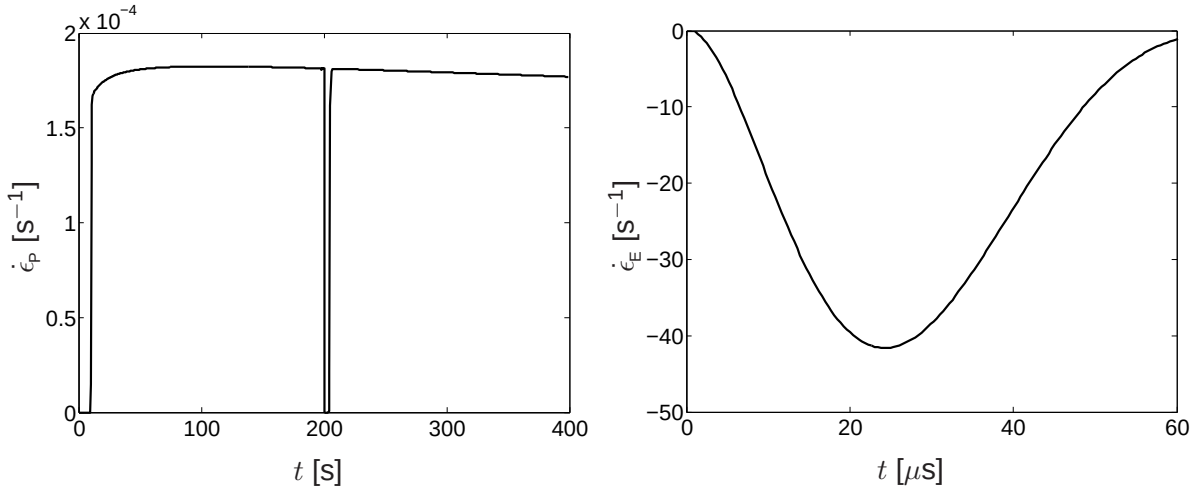

Figure 4: *Rate of change of the accumulated inelastic strain as a function of time during pulsing. Left: The current pulse at 200 s forces the stress state below the activation threshold, resulting in* $\dot{\epsilon}_P = 0$*. Right: Variation in time of* $\dot{\epsilon}_E$ *starting at* $t = 200$ *s (note the difference in timescale)*

To delve into this in more detail, consider the results in Figure 4 for the rate of the accumulated inelastic strain ϵ_P as well as the rate of $\epsilon_E = |\mathrm{dev}(\ln \boldsymbol{V}_E)|$, representing the norm of the deviatoric part of the left logarithmic stretch tensor. As soon as the temperature rises, the spherical part $\mathrm{sph}(\ln \boldsymbol{V}_E)$ of $\ln \boldsymbol{V}_E$ increases (see (11)). Conversely, the deviatoric part and, hence, ϵ_E decreases. Accordingly, since $|\mathrm{dev}(\boldsymbol{K})| = 2\mu\epsilon_E$, the activation stress (9) decreases and elastic unloading can be observed. The drop of $\dot{\epsilon}_P$ to zero takes place within 60 μs (see Figure 4 right). Afterwards, the tensile testing machine continues to load the specimen in the elastic domain for several seconds until the inelastic flow is reactivated. As shown, in this range, $\dot{\epsilon}_P = 0$.

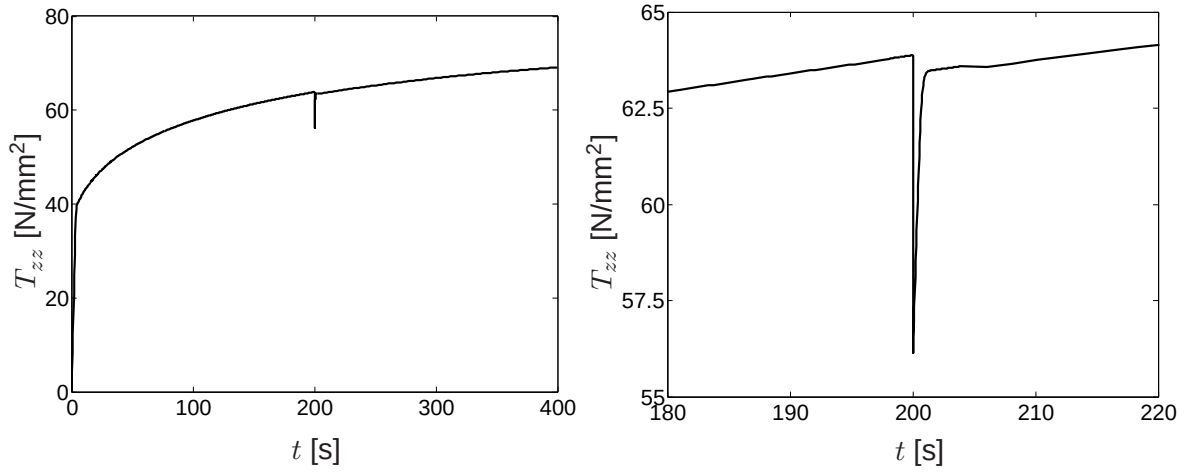

Figure 5: *Simulated stress drop in aluminum due to Joule heating during simple tension. Left: Change of* T_{zz} *with time. Right: Blow-up of the stress drop region in time*

Such testing has also been carried out for technically pure aluminum (*e.g.*Al99,5 or AA1000 series). As all experimental conditions are the same as for the tests with titanium, the particular material characteristics of aluminum are the reason for a smaller stress drop. In particular, for the same geometry and imposed current I, $\boldsymbol{j}$ as given by (3) is the same for both materials. Since the contribution to $\dot{\theta}$ from Joule heating is given by $\det(\boldsymbol{F})\,\boldsymbol{j}\cdot\boldsymbol{j}/(\varrho_r c_r \sigma_{\text{EM}})$ from $(10)_3$ any difference between the two materials is due to the magnitude of $\varrho_r c_r \sigma_{\text{EM}}$. The parameter values in Table 3 imply that the heat capacity per unit volume $\varrho_r c_r$ is comparable in aluminum and titanium. On the other hand, $\sigma_{\text{EM}}^{\text{Al}} = 3.8 \times 10^7$ Ohm^{-1} m^{-1} and $\sigma_{\text{EM}}^{\text{Ti}} = 2.6 \times 10^6$ Ohm^{-1} m^{-1}. Consequently, $\sigma_{\text{EM}}^{\text{Al}} \gg \sigma_{\text{EM}}^{\text{Ti}}$, and it is clear why the temperature rise in aluminum (6 K) is much smaller than that in titanium (50 K). Via the thermoelastic coupling in (11), then, this difference in temperature increase is reflected in the respective stress drops, *i.e.*60 MPa for titanium and 6 MPa for aluminum (Figure 5).

4 Conclusions

For the typical timescales, imposed current densities and materials generally relevant for EMF processes load drops during tensile testing are observed. For titanium and aluminum it was shown that the magnitude of the load drops can be modeled without postulating a direct interaction between electron and dislocation movement. The modeling of experimental results indicate that conventional effects such as Joule heating and thermal expansion are able to explain the experimental observations quite well. Such an interation, if it exists, can be considered to be of second order.

References

[1] *Svendsen, B.* and *Chanda, T.*: Continuum thermodynamic formulation of models for electromagnetic thermoinlastic materials with application to electromagnetic metal forming. Cont. Mech. Thermodyn., vol. 17 p. 1–16, 2005.

[2] *Stiemer, M.*; *Unger, J.*; *Blum, H.* and *Svendsen, B.*: Algorithmic formulation and numerical implementation of coupled electromagnetic-inelastic continuum models for electromagnetic metal forming. Int. J. Numer. Methods Engrg., 2006.

[3] *Lemaitre, J.* and *Chaboche, J.-L.*: Mechanics of solid materials. Cambridge University Press, 1990.

[4] *Conrad, H.* and *Sprecher, A. F.*: The electroplastic effect in metals. In F. R. N. Nabarro, editor, Dislocations in solids, p. 499–541. Elsevier Science Publishers, 1989.

[5] *Varma, S.* and *Cornwell, L. R.*: The Electroplastic Effect in Aluminum. Scripta Metallurgica, vol. 13 p. 733–738, 1979.

[6] *Bilyk, S.*; *Ramesh, K.* and *Wright, T.*: Finite deformations of metal cylinders subjected to electromagnetic fields and mechanical forces. Journal of the Mechanics and Physics of solids, vol. 53 p. 525–544, 2005.

[7] *Troitskii, O. A.*: Electromechanical effect in metals. Zh. Eksp. Teor. Fiz., vol. 10(1) p. 18–22, 1969.

[8] *Molotskii, M.*: Theoretical basis for electro- and magnetoplasticity. Materials Science & Engineering, vol. 287 p. 248–258, 2000.

[9] *Goldman, P. D.*; *Motowidlo, L. R.* and *Galligan, J. M.*: The Absense of an Electroplastic Effect in Lead at 4.2 K. Scripta Metallurgica, vol. 15 p. 353–356, 1980.

[10] *Okazaki, K.*; *Kagawa, M.* and *Conrad, H.*: Effects of strain rate, temperature and interstitial content on the electroplastic effect in titanium. Scripta Metallurgica, vol. 13 p. 473–477, 1979.

[11] *Jackson, J. D.*: Classical Electrodynamics. John Wiley and Sons, 1987.

[12] *Svendsen, B.*: On the modeling of anisotropic elastic and inelastic material behaviour at large deformation. Int. J. Solids Structures, vol. 38 p. 9579–9599, 2001.

[13] *Rosakis, P.*; *Rosakis, A. J.*; *Ravichandran, G.* and *Hodowany, J.*: A thermodynamic internal variable model for the partition of plastic work into heat and stored energy in metals. J. Mech. Phys. Solids, vol. 48 p. 581–607, 2000.

[14] *Teodosiu, C.*: Dislocation modeling of crystalline plasticity. In C. Teodosiu, editor, Large plastic deformation of crystalline aggregates, CISM, p. 21–80. Springer, 1997.